Precision Targeting for Multiple Swingby Interplanetary Trajectories

STEPHEN BAYLISS*
The Aerospace Corporation, El Segundo, Calif.

A rapid technique for precision targeting of multiple swingby interplanetary trajectories is described. The general multiple swingby interplanetary trajectory is modeled as a sequence of alternating heliocentric and planetocentric trajectory segments constrained to match in position and time at each planetary sphere of influence penetration. An iterative procedure is employed to vary these penetration points to match the segments in velocity as well. Effects of *N*-body disturbing accelerations on the trajectory segments are included using a general perturbation technique. Results which indicate a rapid rate of convergence and a high level of accuracy along the entire trajectory without the need for numerical integration are presented for missions with two and three swingbys.

Nomenclature

A_i,B_i,C_i,D_i = submatrices of $\Phi(t_i,t_M)$
$\mathbf{a}_d$ = total disturbing acceleration vector
a_i = semimajor axis of the orbit of planet i
$a_{P,i}$ = acceleration vector due to the sun of planet i
$\mathbf{d}$ = disturbing vector for state perturbation calculation
e = eccentricity of conic trajectory segment
G = universal gravitational constant
$\mathbf{g}$ = combined gradient vector
i = inclination of conic trajectory segment
J = cost function for the degree of velocity mismatch along the trajectory
J_k = individual term in the cost function corresponding to the kth matching point
m_i = mass of the ith planet
N = number of intermediate matching points
$\mathbf{r}$ = position vector
$\mathbf{r}_{P,i}$ = position vector of the ith planet with respect to the sun
$r_{s,i}$ = sphere of influence radius for planet i
$\delta\mathbf{r}$ = position vector offset
$\Delta r(t_i)$ = magnitude of error in position at time t_i
SOI = abbreviation for sphere of influence
T = time of flight for a trajectory segment
t_1,t_2 = initial and final, respectively, time for a trajectory segment
t_k = time associated with the kth matching point
t_M = midpoint time for a trajectory segment
$\mathbf{v}$ = velocity vector
$\mathbf{v}_{E,k}$ = velocity (relative to the sun) on heliocentric (usually elliptic) arc at the kth matching point
$\mathbf{v}_{H,k}$ = velocity (relative to the planet) on a planetocentric (always hyperbolic) arc at the kth matching point
$\mathbf{v}_{P,k}$ = velocity (relative to the sun) of the planet associated with the kth matching point at time t_k
$\Delta\mathbf{v}$ = combined velocity discontinuity vector
$\Delta\mathbf{v}_k$ = velocity discontinuity vector at the kth matching point
$\Delta\mathbf{v}(t_1),\Delta\mathbf{v}(t_2)$ = errors in calculated initial and final velocity for a trajectory segment
$\delta\mathbf{v}$ = velocity vector offset
$\mathbf{x}$ = combined matching point coordinate vector
$\mathbf{x}_j$ = coordinate vector specifying jth matching point
$\mathbf{y}$ = state vector = $[\mathbf{r},\mathbf{v}]^T$
$\delta\mathbf{y}$ = state vector offset
μ = gravitational parameter (Gm) of the sun
μ_i = gravitational parameter (Gm_i) of planet i
τ = dummy time variable
θ_k = celestial longitude of the kth matching point
φ_k = celestial latitude of the kth matching point
$\Phi(t_i,t_j)$ = two-body state transition matrix between times t_i and t_j
∇_j = gradient operator $(\partial/\partial\mathbf{x}_j)$
$(\ )^T,(\ )^{-1}$ = vector transpose and vector inverse, respectively
$(\hat{\ })$ = new value for a vector after the perturbed conic analysis

Presented as Paper 71-191 at the AIAA 9th Aerospace Sciences Meeting, New York, January 25-29, 1971; submitted February 8, 1971; revision received June 9, 1971. This paper summarizes work done as a Ph.D. thesis[1] in the Department of Aeronautics and Astronautics at the Massachusetts Institute of Technology.

Index category: Lunar and Planetary Trajectories.

* Member of Technical Staff, Mission Analysis Department. Associate Member AIAA.

Introduction

MOST recent studies[2,3] involving multiple swingby interplanetary trajectories have been made using a simplified model consisting of a sequence of heliocentric conic arcs matched in relative hyperbolic excess velocity at each planetary encounter. This model provides adequate results for preliminary mission analysis, but as more detailed investigations are undertaken an accurate many-body reference trajectory becomes necessary. Present targeting techniques,[4] which usually involve repeated numerical integration of the trajectory, can become time consuming due to the high sensitivity of this nonlinear problem. This paper presents a technique for significantly reducing the computational effort needed to determine a precision reference trajectory.

Conic Analysis

The gap between the simple patched conic model and the integrated N-body trajectory is bridged in two intermediate steps. The first of these involves a more accurate conic model. This consists of breaking up the trajectory into a series of alternating heliocentric and planetocentric conic arcs. These arcs are specified by the position and time of the entry and exit points on the sphere of influence (SOI) of each planet encountered. For example, a heliocentric arc runs from the exit point of the SOI of planet k to the entry point of the SOI of planet $k+1$ while a planetocentric arc runs from the entry point to the exit point of the SOI for the single planet k. Since the end points and the time of flight are given for each conic arc, the initial and final velocities may be calculated by solving Lambert's problem.[5] Having based the initial guess at the entry and exit points on an approximate model, these velocities are not likely to match. Instead, velocity discon-

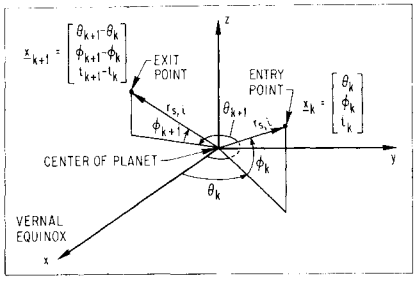

Fig. 1 Description of ecliptic coordinate system used to specify entry and exit points on the sphere of influence.

tinuities are expected at each entry and exit point. Let these be represented by

$$\Delta \mathbf{v}_k = \mathbf{v}_{E,k} - \mathbf{v}_{P,k} - \mathbf{v}_{H,k} \tag{1}$$

The coordinate system defining the matching points at each planet is shown in Fig. 1. The kth entry point is specified by its Julian Date of arrival (t_k) and its celestial latitude (φ_k) and longitude (θ_k) in an inertial, planet-centered, ecliptic coordinate system. The exit point is defined by the differences in celestial latitude and longitude and time from the entry point to the exit point. This coordinate system definition was chosen to provide some separation in the effects of varying the matching points. The two heliocentric arcs touching a planet's SOI are affected primarily by changes in the entry point while the planetocentric arc inside the SOI is affected primarily by changes in the exit point. Both the entry and exit points are constrained to lie on the surface of a planet-centered sphere whose radius is given by

$$r_{s,i} = a_i(\mu_i/\mu)^{1/3} \tag{2}$$

This definition results in a somewhat larger sphere of influence than is normally used. Work by Carlson[6] indicates that this is the best choice for a region of overlapping validity of the heliocentric and planetocentric trajectory representations.

From the results of the solution of Lambert's problem for each of the conic arcs, it is possible to define a scalar cost function for the degree of velocity mismatch of the arcs as

$$J = \sum_{k=1}^{N} \Delta \mathbf{v}_k{}^T \Delta \mathbf{v}_k = \sum_{k=1}^{N} J_k \tag{3}$$

From differentiation of the relations for the solution of Lambert's problem, analytic expressions for the following gradient matrices may be obtained

$$\nabla_j \mathbf{v}_{E,k} = \partial \mathbf{v}_{E,k}/\partial \mathbf{x}_j \tag{4}$$

$$\nabla_j \mathbf{v}_{H,k} = \partial \mathbf{v}_{H,k}/\partial \mathbf{x}_j \tag{5}$$

where $\mathbf{x}_j$ is the state vector (latitude, longitude, and time) of the jth matching point. The only nonzero components of $\nabla_k \mathbf{v}_{P,j}$ are approximated by

$$\partial \mathbf{v}_{P,k}/\partial t_k = \mathbf{a}_{P,i}(t_k) = -(\mu_i/r_{P,i}{}^3)\mathbf{r}_{P,i}(t_k) \tag{6}$$

The complete derivation of Eqs. (4) and (5) is given in Ref. 1. In general, the gradient matrices indicate a proportionately higher sensitivity with respect to t_j than with respect to θ_j or φ_j. Also, the matrices for the planetocentric arcs indicate more sensitivity than those for the heliocentric arcs for equal changes in trajectory endpoints. The coordinate system chosen alleviates problems due to this effect to a great extent. Having computed these gradient matrices, one may write the gradient of each of the cost function terms with respect to any of the matching points as

$$\partial J_k/\partial \mathbf{x}_j = 2\Delta \mathbf{v}_k{}^T(\nabla_j \mathbf{v}_{E,k} - \nabla_j \mathbf{v}_{P,k} - \nabla_j \mathbf{v}_{H,k}) \tag{7}$$

These terms may be combined to form the gradient vector $\mathbf{g} = \partial J/\partial \mathbf{x}$ of the cost function given in Eq. (3) with respect to a vector

$$\mathbf{x}^T = [\mathbf{x}_1, \mathbf{x}_2, \ldots, \mathbf{x}_N] \tag{8}$$

made up of all the matching points. Having this gradient vector, one may use any of the standard first-order techniques to vary the matching points to minimize the cost function J. The method chosen was a modified form of the steepest descent procedure given in Ref. 7. The modification adds an adaptive weighting matrix which biases the direction of the step in favor of those components of the gradient which do not change sign on successive steps. This procedure helps eliminate a severe ravine problem caused by the differing sensitivities of the gradient to changes in the time and angular components of $\mathbf{x}$. The steepest descent method yields large reductions in the cost function in the first few steps but has poor convergence characteristics in the neighborhood of the minimum.

An alternative method (Newton-Raphson[8]) is to form the set of linear equations

$$-\Delta \mathbf{v} = [\partial \Delta \mathbf{v}/\partial \mathbf{x}]\Delta \mathbf{x} \tag{9}$$

where

$$\Delta \mathbf{v}^T = [\Delta \mathbf{v}_1, \Delta \mathbf{v}_2, \ldots, \Delta \mathbf{v}_N] \tag{10}$$

$$\Delta \mathbf{x}^T = [\Delta \mathbf{x}_1, \Delta \mathbf{x}_2, \ldots, \Delta \mathbf{x}_N] \tag{11}$$

and the matrix $[\partial \Delta \mathbf{v}/\partial \mathbf{x}]$ is built up from the gradient matrices given in Eq. (4–6). Since changes in a matching point affect only those arcs near that point, this matrix is a banded matrix for which storage requirements and inversion time may be considerably reduced. After inversion of this matrix, Eq. (9) may be solved for the changes $\Delta \mathbf{x}$ in the matching points needed to reduce all the $\Delta \mathbf{v}_k$ to zero. This technique exhibits second-order convergence properties. For all numerical examples examined for which a solution $\Delta \mathbf{v} = \mathbf{0}$ existed, the Newton-Raphson procedure encountered no convergence difficulties. For examples where the cost function had a nonzero minimum, only the steepest descent technique was employed.

Perturbed Conic Analysis

Having converged to a minimum (or zero) of the cost function J for the conic model, a second intermediate step using a perturbed conic model is employed. Up to this point, each trajectory segment has been considered to be a simple two-body orbit. In the perturbed conic model, the perturbing effects of the sun on the planetocentric legs and the effects of the planets on the heliocentric legs are included.

Starting from the midpoint of each conic leg, the perturbations in position and velocity due to the disturbing bodies are computed going backward in time to the initial point and forward in time to the final point. These perturbations are evaluated using

$$\delta \mathbf{y}(t_1) = \begin{bmatrix} \delta \mathbf{r}(t_1) \\ \delta \mathbf{v}(t_1) \end{bmatrix} = \int_{t_M}^{t_1} \Phi(t_1,\tau)\mathbf{d}(\tau)d\tau \tag{12}$$

$$\delta \mathbf{y}(t_2) = \begin{bmatrix} \delta \mathbf{r}(t_2) \\ \delta \mathbf{v}(t_2) \end{bmatrix} = \int_{t_M}^{t_2} \Phi(t_2,\tau)\mathbf{d}(\tau)d\tau \tag{13}$$

where

$$\mathbf{y}^T = [\mathbf{r}, \mathbf{v}] \tag{14}$$

is the state vector, and

$$\mathbf{d}^T = [\mathbf{0}, \mathbf{a}_d(t)] \tag{15}$$

This process is illustrated schematically in Fig. 2. Both the state transition matrix $\Phi(t,t_i)$ and the disturbing acceleration $\mathbf{a}_d(t)$ are evaluated along the nominal conic arc. Thus the

integrands in Eq. (12) and (13) may be calculated purely as functions of time and the integrals evaluated by quadrature using a method such as Simpson's Rule.

Once the position and velocity perturbations at both ends of the conic arc have been evaluated, the next step is to solve for the midpoint offset in position and velocity that causes zero position deviation at the initial and final times. The new initial and final perturbations corresponding to this midpoint offset are

$$\delta\hat{\mathbf{y}}(t_1) = \begin{bmatrix} 0 \\ \delta\hat{\mathbf{v}}(t_1) \end{bmatrix} = \Phi(t_1,t_M)\delta\,\hat{\mathbf{y}}(t_M) + \delta\mathbf{y}(t_1) \quad (16)$$

and

$$\delta\hat{\mathbf{y}}(t_2) = \begin{bmatrix} 0 \\ \delta\hat{\mathbf{v}}(t_2) \end{bmatrix} = \Phi(t_2,t_M)\ \delta\hat{\mathbf{y}}(t_M) + \delta\mathbf{y}(t_2) \quad (17)$$

This required midpoint offset may be determined using

$$\delta\hat{\mathbf{y}}(t_M) = \begin{bmatrix} A_1 & B_1 \\ A_2 & B_2 \end{bmatrix}^{-1} \begin{bmatrix} -\delta\mathbf{r}(t_1) \\ -\delta\mathbf{r}(t_2) \end{bmatrix} \quad (18)$$

where the state transition matrix has been partitioned into

$$\Phi(t_1,t_M) = \begin{bmatrix} A_1 & B_1 \\ C_1 & D_1 \end{bmatrix} \quad (19)$$

$$\Phi(t_2,t_M) = \begin{bmatrix} A_2 & B_2 \\ C_2 & D_2 \end{bmatrix} \quad (20)$$

Then, using Eqs. (16) and (17), the initial and final velocity offsets necessary for a perturbed trajectory which passes through the same initial and final conditions in position and time as the nominal conic arc may be determined. This trajectory is illustrated schematically in Fig. 3.

Two factors combine to make this procedure for the determination of the velocity offsets feasible. First, since the calculations for the perturbed trajectories always run from regions of weak perturbations (the midsection of each trajectory arc) to regions of strong perturbations (the end points), large deviations (due to the accumulated effects of the strong perturbations) do not have time to grow. Also, since the effects of the strong perturbing forces depend primarily on the time spent in the vicinity of the SOI boundaries at the end points rather than on the time of flight of the trajectory, the size of the offsets is not influenced heavily by the length of the trajectory. Second, the choice of the enlarged SOI [see Eq. (2)] allows the use of the two-body state transition matrix in the perturbations calculation. Numerical studies comparing an analytic two-body state transition matrix formulation[9] with a many-body state transition matrix determined by numerical integration show that terms in both matrices remain within a few percent of each other for both heliocentric and planetocentric legs when this enlarged SOI is used. When the more commonly employed Laplace SOI [defined by $r_{s,i} = a_i(\mu_i/\mu)^{2/5}$] is used, large differences (often over 100%) occur in terms in the C and D submatrices for the heliocentric legs.

Table 1 Computed values of the initial and final velocity offsets for each trajectory leg, the errors in these velocity offsets, and the final position error that would result from the initial velocity offset error for the dual planet reconnaissance trajectory

Lag	Initial velocity offset $[\delta v(t_1)]$, m/sec	Error $[\Delta v(t_1)]$, m/sec	Final velocity offset $[\delta v(t_2)]$, m/sec	Error $[\Delta v(t_2)]$, m/sec	Final position error $[\Delta r(t_2)]$, km
Earth-Venus	34.286	0.1250	24.139	0.0450	5327.23
Venus	19.034	0.0030	14.558	0.0091	9.71
Venus-Mars	22.322	0.0430	3.211	0.0041	1306.70
Mars	2.221	0.0028	2.183	0.0030	1.62
Mars-Earth	2.997	0.0017	14.982	0.0173	15.39

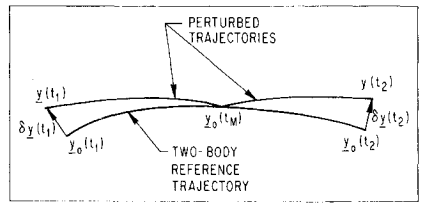

Fig. 2 Schematic representation of state offset calculation procedure, step 1.

It is now possible to construct an iterative process to converge on a set of perturbed conic arcs which match in velocity. The steps in this process are listed below.

1) Recompute the cost function J using the perturbed values of $\mathbf{v}_{E,k}$ and $\mathbf{v}_{H,k}$ (i.e., conic values plus offsets).

2) Neglecting the effects of changes in the matching points on the values for the velocity offsets, use the minimization techniques described previously to find a new set of matching points which minimizes the perturbed cost function.

3) Recompute the velocity offsets for this new set of matching points and re-evaluate the perturbed cost function using these offsets. If the difference between the old and new values for the cost function is neglible, terminate the iteration. Otherwise, go back to step 2.

Having converged on a solution for the perturbed conic step which reduces the cost function to zero, the resulting multiple swingby trajectory consists of a sequence of perturbed conic arcs matched in position, velocity, and time at every SOI penetration point. At this point, two alternative procedures are possible.

1) Each trajectory leg may be targeted individually using numerical integration to get improved values for the initial and final velocity offsets for each leg. An iterative procedure similar to the one described for the perturbed conic step may be used to converge to a new solution for the matching points. The result of this alternative would be a sequence of numerically integrated trajectory legs matched in position, velocity, and time at each SOI penetration point. The accuracy of the solution would be equal to the accuracy with which any single trajectory leg could be determined. It is estimated that two to three cycles of the aforementioned procedure (each involving two to three integrations of each individual trajectory leg) would be required to converge to this solution.

2) The accuracy of the perturbed conic analysis may be accepted as sufficient for the intended application. If a check on this accuracy is desired, each individual trajectory leg may be targeted once using numerical integration and the true remaining velocity mismatch for the given set of matching points may be determined. These velocity differences may then be considered known quantities to be absorbed into the midcourse corrections at the matching points.

Since the magnitudes of the velocity differences remaining after the perturbed conic analysis are small (usually less than

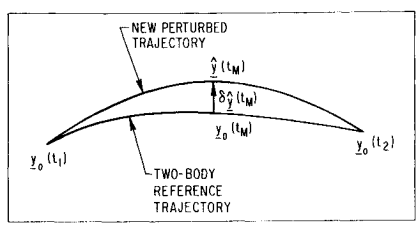

Fig. 3 Schematic representation of state offset calculation procedure, step 2.

1 m/sec), the second procedure is the one used for the examples in this paper.

Numerical Results

Dual Planet Reconnaissance Trajectory

This mission employs a free-fall trajectory which leaves Earth, makes a close pass first by Venus (periapse altitude = 1.39 planetary radii) and then by Mars (periapse altitude = 1.94 planetary radii), and then returns to Earth. Total time of flight is about 1.3 years. Using the planetary encounter dates determined in Battin,[5] a simple patched conic model is employed to calculate a first guess for the SOI entry and exit point coordinates. Then, the procedure described above is used to generate the sequence of matching perturbed conic heliocentric and planetocentric legs making up the trajectory. The total running time required to converge to the final solution was 48 sec on the IBM 360/65.

The accuracy of the reference trajectory generated is evaluated by comparison with numerically integrated trajectory legs determined using the following procedure.

1) The initial conditions for the numerical integration are set equal to the conic position and the perturbed conic velocity (i.e., conic value plus initial velocity offset) at the initial time t_1.

2) The many-body equations of motion and the differential equations for the many-body state transition matrix are integrated forward to the final time t_2. The deviations in position $\Delta\mathbf{r}(t_2)$ and velocity $\Delta\mathbf{v}(t_2)$ from the conic position and perturbed conic velocity at the final time t_2 are calculated.

3) Using the many-body state transition matrix between t_1 and t_2, the velocity correction $\Delta\mathbf{v}(t_1)$ needed to eliminate $\Delta\mathbf{r}(t_2)$ is applied to the initial velocity at t_1.

Steps 2 and 3 are repeated until $\Delta\mathbf{r}(t_2)$ is drive to zero. If the initial guess is close, this happens quite rapidly. For the examples considered, $\Delta\mathbf{r}(t_2)$ was reduced to under 10^{-5} km in two iterations.

The magnitudes of $\Delta\mathbf{v}(t_1)$ and $\Delta\mathbf{v}(t_2)$ for each converged numerically integrated trajectory leg as well as the magnitude of $\Delta\mathbf{r}(t_2)$ for the first iteration (i.e., before any correction has been applied to the initial velocity) are given in Table 1. Since $\Delta\mathbf{v}(t_1)$ and $\Delta\mathbf{v}(t_2)$ may be considered to be the errors in the velocity offset calculation, the magnitude of the initial and final offsets are included for comparison. In all cases, these errors represent less than one to two percent of the offset magnitude. The size of $\Delta\mathbf{r}(t_2)$ indicates the importance of the initial velocity offset error. The small size of this quantity indicates that the velocity errors are in a nonsensitive direction as well as being small in magnitude.

Grand Tour Trajectory

This mission employs a free-fall trajectory which leaves the Earth and makes successive close passes by Jupiter (periapse altitude = 21.63 planetary radii), Saturn (periapse altitude = 1.43 planetary radii), Uranus (periapse altitude = 4.92 planetary radii), and Neptune. Total flight time is about 10.8 years. The initial guess for the SOI entry and exit point coordinates was generated using the planetary encounter dates given by Silver.[2] The total running time required to converge to the final solution was 172 sec on the IBM 360/65.

The accuracy of the Grant Tour reference trajectory generated was evaluated in the same manner used in the preceding example. The results are given in Table 2. In this example, all the errors in the velocity offset calculation are less than one percent of the offset values. The assumption that the disturbing acceleration due to other planets has negligible effect during the planetocentric legs of the trajectory does not prove to be as good for this example as it did for the dual planet reconnaissance trajectory. This shows up most strongly for the planetocentric leg at Saturn where the long time inside the SOI (196 days), the low periapse altitude (1.43 planetary radii), and the proximity of Jupiter (about 5 a.u. away) cause larger offset errors and a much larger value of $\Delta r(t_2)$ than would be expected. If the disturbing accelerations due to the other planets are ignored in the numerical integration of the Saturn leg, the offset errors become $\Delta v(t_1) = 0.026$ m/sec and $\Delta v(t_2) = 0.004$ m/sec and the final position error is $\Delta r(t_2) = 1705$ km. The same error sources are present in the Jupiter leg but the higher periapse altitude (21.63 planetary radii) prevents the offset errors from having such a strong effect on $\Delta r(t_2)$. Both of these examples are discussed in greater detail in Ref. 1.

Table 2 Computed values of the initial and final velocity offsets for each trajectory leg, the errors in these velocity offsets, and the final position error that would result from the initial velocity offset error for the Grand Tour trajectory

Leg	Initial velocity offset $[\delta v(t_1)]$, m/sec	Error $[\Delta v(t_1)]$, m/sec	Final velocity offset $[\delta v(t_2)]$, m/sec	Error $[\Delta v(t_2)]$, m/sec	Final position error $[\Delta r(t_2)]$, km
Earth-Jupiter	16.800	0.305	92.557	0.139	8185.05
Jupiter	94.702	0.622	81.347	0.438	8955.75
Jupiter-Saturn	100.210	0.353	10.165	0.089	15,348.52
Saturn	34.431	0.335	20.439	0.184	239,662.60
Saturn-Uranus	42.388	0.052	14.480	0.095	6444.35
Uranus	2.820	0.0081	2.104	0.0071	1904.25
Uranus-Neptune	10.560	0.095	9.195	0.095	8833.50

Conclusions

The basic advantages of the trajectory targeting technique developed in this paper are: 1) The technique is basically analytic in nature, providing a great reduction in required computation. Its convergence range is wide. 2) A continuous description of the entire trajectory is provided. The near-planet phases of the trajectory are approximated quite well by the planetocentric legs, and 3) By specifying the trajectory as a sequence of individual legs matched in position, velocity, and time, the determination of the trajectory is uniformly accurate along its entire length.

The main limitation of the analytic technique lies in its accuracy. The primary assumption of the perturbation techniques employed is that each trajectory segment is two-body in nature. The presence of strong disturbing accelerations acting over extended periods of time can cause larger perturbations from the two-body reference orbits and lead to a degradation of the accuracy of the results. In such cases, the use of a final stage employing numerical integration to calculate the velocity offsets (for the strongly perturbed legs only) may be necessary.

The basic conclusion of this paper is that the analytic targeting technique presented in this paper provides sufficiently accurate results for a wide variety of multiple swingby missions. Where its accuracy is not adequate, it may be supplemented by a final stage using numerical integration (with the associated penalty of increased computational time) to provide any degree of accuracy required. For heliocentric arcs, initial and final velocities may be determined to better than 0.4 m/sec. Errors in final position for a numerical integration of each leg using the calculated initial velocity range from 1300 km to 15,000 km with typical values falling in the region of 5000–8000 km. For planetocentric arcs, the initial and final velocities are determined to within 0.1 m/sec. Exceptions to this occur at Jupiter and Saturn for the Grand

Tour example where the neglected effects of the disturbing acceleration due to other planets proved significant. Errors in final position for numerical integration of individual legs using the calculated initial velocity range from 1.6 km to 240,000 km with the bulk of the values in the 2–2000 km interval.

References

[1] Bayliss, S. S., "Precision Targeting for Multiple Swingby Interplanetary Trajectories," TE-39, June 1970, Measurement Systems Lab., MIT, Cambridge, Mass.

[2] Silver, B., "Grand Tours of the Jovian Planets," *Journal of Spacecraft and Rockets*, Vol. 5, No. 6, June 1968, pp. 633–637.

[3] Vanderveen, A., "Triple Planet Ballistic Flybys of Mars and Venus," *Journal of Spacecraft and Rockets*, Vol. 6, No. 4, April 1969, pp. 383–389.

[4] Sturms, F., "Trajectory Analysis of an Earth-Venus-Mercury Mission in 1973," TR-32-1062, Jan. 1967, Jet Propulsion Lab., Pasadena, Calif.

[5] Battin, R., *Astronautical Guidance*, McGraw-Hill, New York, 1964, pp. 75–82, 169–171.

[6] Carson, N., "An Explicit Analytic Guidance Formulation for Many-Body Space Trajectories," TE-30, May, 1969, Measurement Systems Lab., MIT, Cambridge, Mass., pp. 90.

[7] Bryson, A. and Ho, Y., *Applied Optimal Control*, Blaisdell, Waltham, Mass., 1969, pp. 19–21.

[8] Hildebrand, F., *Introduction to Numerical Analysis*, McGraw-Hill, New York, 1956, pp. 447–451.

[9] Goodyear, W., "A General Method for the Computation of Cartesian Coordinates and Partial Derivatives of the Two-Body Problem," CR-522, Sept. 1966, NASA.

SEPTEMBER 1971 J. SPACECRAFT VOL. 8, NO. 9

Analysis of Mariner VII Pre-Encounter Anomaly

H. J. GORDON,* S. K. WONG,† AND V. J. ONDRASIK‡
Jet Propulsion Laboratory, Pasadena, Calif.

The loss of signal at 127 hr before closest approach to Mars and the subsequent changes in the spacecraft and in its trajectory are described. Real-time orbit determination activity as well as postencounter analysis are discussed. Great difficulty was experienced in processing tracking data influenced by an unknown nongravitational force that could not be properly modeled. Results of simulations using known perturbations are presented. It is concluded that the battery case had ruptured and vented into the interior of the spacecraft. This rupture caused corona discharges, and escaping gas produced the translational forces.

Introduction

AT 127 hr before Mariner VII was scheduled to encounter Mars, its radio signal was lost abruptly. When the signal was reacquired after 7 hr and 12 min, the doppler tone showed that the radial velocity had decreased by 1.89 cm/sec. There was no further change in velocity for 71 min, at which time two-way lock was lost again for 60 min; when reacquired, it showed that the radial velocity had decreased by an additional 0.78 cm/sec. The radial velocity continued to decrease at an apparently exponentially decaying rate during the next two weeks. This meant that the orbit had to be redetermined in less than five days (in the presence of a nongravitational force that was not modeled in the orbit determination programs) so that all science instruments could be optimally pointed during the encounter.

Orbit Determination

Orbit determination is done by an iterative, weighted, least-squares method that assumes Gaussian random errors superimposed on the tracking data as well as on the initial estimates. Reference 1 describes the basic concepts; Ref. 2 describes the single precision orbit determination program. (A double precision orbit determination program, DPODP, was constructed and used for the first time during the Mariner 69 operations.) The common types of data and their associated accuracies are shown in Table 1 and more fully described in Ref. 3.

A linearized coordinate system has been adopted to express the terminal coordinates of an interplanetary trajectory. This coordinate system, as described by Kizner,[4] is illustrated in Fig. 1. The terminal coordinates can be defined as $\mathbf{B}\cdot\mathbf{R}$ and $\mathbf{B}\cdot\mathbf{T}$ or as B and θ, where θ is the angle measured clockwise from $\mathbf{T}$ to $\mathbf{B}$ with the time of closest approach (T_{CA}).

Pre-Anomaly Orbits

Figure 2 shows the results of processing different lengths of data arcs, using different data types (doppler only or doppler plus range), and estimating different sets of parameters. The $\mathbf{B}\cdot\mathbf{R}$ and $\mathbf{B}\cdot\mathbf{T}$ coordinates are plotted, and the tight clus-

Table 1 Data types and accuracies

Data type	Measurement accuracy (1σ)	Comments
Two-way doppler	0.01 Hz = 0.7 mm/sec	Measures radial velocity
Three-way doppler	0.01 Hz = 0.7 mm/sec	Bias is typically 0.2 Hz
Mar IA range	35 m	Ground and spacecraft delay contribute
Planetary range	15 m	Ground and spacecraft delay contribute

Presented as Paper 70-1065 at the AAS/AIAA Astrodynamics Conference, Santa Barbara, Calif., August 19–21, 1970; submitted September 28, 1970; revision received March 26, 1971. This paper presents the results of one phase of research carried out at the Jet Propulsion Laboratory, California Institute of Technology, under Contract NAS 7-100, sponsored by NASA.

Index categories: Lunar and Planetary Trajectories; Spacecraft Navigation, Guidance and Flight-Path Control Systems.

* Member of the Technical Staff, Navigation and Mission Design Section, Jet Propulsion Laboratory, California Institute of Technology. Associate Fellow AIAA.

† Senior Research Engineer, Tracking and Orbit Determination Section.

‡ Senior Engineer, Tracking and Orbit Determination Section.